Molecular interactions of glucocorticoid and mineralocorticoid receptors define novel transcription and biological functions

Tatsuya Sueyoshi[1] [ORCID], Maria G. Petrillo[1], Christine M. Jewell[1] [ORCID], Carl D. Bortner[2], Lalith Perera[3], Xiaojiang Xu[4,5], Felipe I. Aguayo[1] [ORCID], David Diaz-Jimenez[1], Anastasia G. Robinson[1], Molly E. Cook[6], Robert H. Oakley[1], and John A. Cidlowski[1,*]

From the [1]Molecular Endocrinology Group, Signal Transduction Laboratory, NIEHS, NIH, DHHS, Raleigh, North Carolina, USA; [2]Flow Cytometry Center, NIEHS, NIH, DHHS, Raleigh, North Carolina, USA; [3]Computational Chemistry & Molecular Modeling Support Group, Genomic Integrity & Structural Biology Laboratory, NIEHS, NIH, DHHS, Raleigh, North Carolina, USA; [4]Integrative Bioinformatics Group, NIEHS, NIH, DHHS, Raleigh, North Carolina, USA; [5]Department of Pathology and Laboratory Medicine, Tulane University School of Medicine, New Orleans, Louisiana, USA; [6]Epigenomics and DNA Sequence Core Facility, NIEHS, NIH, DHHS, Raleigh, North Carolina, USA

Glucocorticoids are primary stress hormones necessary for life that function to maintain homeostasis. These hormones and their synthetic derivatives are widely used in the clinic to combat disease but are limited by development of resistance and by severe side effects. Understanding how glucocorticoids signal is crucial for developing safer and more effective glucocorticoids. Mechanistically glucocorticoid ligands induce glucocorticoid receptor (GR) homodimerization and regulation of gene expression. Here, we show that GR and mineralocorticoid receptor (MR) form molecular complexes with distinct transcriptional responses that alter the biological roles of GR. MR inhibited GR interaction with genomic DNA and diminished glucocorticoid-regulated gene expression as well as suppressed cell apoptosis induced by GR signaling. Provocatively, multiple therapeutic glucocorticoids differentially induced the GR–MR interaction revealing unknown drug effects that are exploitable for fine-tuning glucocorticoid drug treatments. Molecular modeling of the GR–MR complex predicted an interaction interface residing in the LBD of both GR and MR. Mutation of a key amino acid in the interface of GR compromised GR–MR interaction without affecting GR activity in a gene reporter assay. Overall, our findings uncovered unique crosstalk mechanisms between distinct nuclear receptors providing a novel mechanism of diversity in the action of glucocorticoids that may contribute to context-dependent GR signaling in human health and disease.

Glucocorticoids are primary stress hormones necessary for life. Released in a circadian manner and in response to stress by activation of the hypothalamic–pituitary–adrenal axis, these hormones regulate numerous physiological processes including immune function, metabolism, cardiovascular function, behavior, and cognition in an effort to maintain homeostasis (1–9). Glucocorticoids and their synthetic derivatives are widely used in the clinic for their immunosuppressive and anti-inflammatory actions. Unfortunately, the therapeutic benefit of glucocorticoids is limited by the development of tissue-specific resistance and adverse side effects such as osteoporosis, diabetes, growth inhibition in children, hypertension, anxiety, and depression. Understanding the mechanisms by which tissues and cells differentially respond to glucocorticoids is crucial for developing new glucocorticoids and treatment regimens with improved efficacy and specificity profiles.

The majority of the glucocorticoid action is known to occur through its direct binding with the glucocorticoid receptor (GR), a member of the nuclear receptor superfamily (9–12) which contains 48 distinct transcription factors. It is well known that GR and other nuclear receptor family members regulate their target genes by forming homodimers on regulatory DNA elements. This process in which a ligand activates a specific target nuclear receptor is unlikely to explain the wide range of biological processes regulated by GR. GR activation is well known to beget "context-dependent" consequences including sex, organ, developmental stage, hormonal environment, etc. affect the processes of gene regulation (13–19). These observations raise the possibility of GR functional and physical interactions with other factors including other nuclear receptor family members in terms of gene regulation.

GR and MR are believed to have evolved from a common ancestor molecule based on the similarity of their molecular architectural and protein primary structures (10). GR and MR are each known to form homodimers as active forms after binding with their ligands implying their common ancestor molecules also formed homodimers after the ligand binding. Therefore, we hypothesized that GR and MR may form a heterodimer as a possible signaling mechanism for generating greater diversity in glucocorticoid responses. More than

* For correspondence: John A. Cidlowski, cidlows1@niehs.nih.gov.

Novel interactions of GR and MR in cells and animals

25 years ago, DNA binding–dependent heterodimer formation between GR and MR was observed based on *in vitro* experiments which showed that GR and MR could bind the same glucocorticoid regulatory elements (20–24). Since then, several laboratories have also proposed that GR–MR heterodimer regulates genes in various cell systems and animal tissues (25–31). However, none of these studies have provided direct evidence showing GR–MR molecular interaction in the glucocorticoid responsive cells and the functional and physiological roles of the heterodimers. Our recent findings in transgenic mice suggest GR and MR have functional interactions *in vivo* (32–35). Mice with cardiomyocyte-specific GR KO spontaneously developed cardiac hypertrophy and died prematurely from heart failure. In contrast, mice lacking both GR and MR in the heart did not. These findings suggest that signaling pathways through GR and MR that regulate heart physiology are functionally intertwined (32). Furthermore, neurodegeneration of the hippocampus was observed in mice with conditional KO of both GR and MR but not in the GR or MR single KOs (33). Synergistic increases in the number of dysregulated genes in the hippocampus were observed in double KO compared with single KO counterparts indicating that the functional interaction of these two receptors plays a critical role in the normal physiology of the hippocampus (33).

Here, we identify novel biological functions that depend on the GR and MR interaction in cells using newly established human cell lines stably expressing both of these receptors. Our studies show that GR and MR interact in the cells, and details of their cooperative gene regulation were analyzed at the global level. The results indicate that MR suppresses GR's ability to regulate genes including those related to apoptosis (36). Apoptosis analyses revealed that MR expression attenuated dexamethasone (DEX)-induced apoptosis of GR-expressing cells. Furthermore, we show that GR and MR interact within a few minutes after the addition of selective GR or selective MR ligands using a newly developed method for monitoring the heterodimer formation in living cells. Based on the MR ligand-binding domain (LBD) dimer structure in the protein crystal (37), we propose a model structure for GR-MR LBD heterodimers. We also demonstrate that therapeutic glucocorticoids induced the heterodimer to different degrees providing a mechanistic rationale for selectivity in their activities. Thus, we uncover for the first time that gene regulation activity of GR is modulated by MR through direct interaction which results in the alteration of biological responses of the cells. GR–MR heterodimers can coexist with their homodimer counterparts simultaneously and the ratio between homodimers and heterodimers may modulate a wide variety of biological responses in animal tissues resulting in "context-dependent" GR activation. Taken together, these discoveries provide a foundation for future research about biological functions played by heterodimers between GR and MR in mammalian physiology and contribute to developing new glucocorticoids for treating human inflammatory diseases.

Results

GR functionally interacts with MR for novel gene regulation in heart and hippocampus

We previously demonstrated that global gene expression in heart and hippocampus is highly dependent on the presence of both GR and MR (32, 33, 35). Venn diagrams in Figure 1A summarize our analysis of gene expression changes that occur by knocking out GR, MR, or both GR and MR in these organs. The numbers in the diagram indicate the number of genes with significant changes in their expressions in the gene array studies (32, 33). We observed a total of 565, 449, and 856 differentially regulated genes (DEGs) in heart or 413, 1478, and 3637 DEGs in hippocampus in GR knockout mice, MR knockout mice, and GR and MR double KO, respectively. Comparison of the DEGs in the different mouse models suggests a major role for the cooperative actions of GR and MR since a large number of genes are uniquely altered only when both receptors are depleted in the heart (649 genes) and hippocampus (2438 genes). These findings prompted us to examine the potential molecular interaction of these receptors and other members of the nuclear receptor family.

Establishing GR, MR, and MR/GR U-2OS cell lines

As the first step for elucidating the molecular mechanisms and potential biological functions of GR–MR interaction in mammalian cells, we developed cell lines that stably express GR (GR cell line), MR (MR cell line), or both (MR/GR cell line) using U-2OS, a human osteosarcoma–derived cell line, as the host employing the transfection and screening strategy described in the Experimental procedures and depicted in Figure 1B. U-2OS has been used extensively to investigate glucocorticoid signaling mechanisms and has well-defined glucocorticoid responses (36). Therefore, this human cell line can be utilized as a host for appropriate model systems for studying gene regulation and biological responses caused by the interaction of GR and MR. Protein and mRNA in these cell lines were analyzed and shown in Figure 1, *C* and *D*. Western blotting analyses in Figure 1D revealed that GR and MR protein expression levels correlated well with mRNA expression levels (Fig. 1C). Compared to U-off cell line, GR protein levels were ≈9.5-fold higher in GR and MR/GR cell lines, whereas MR protein levels were ≈4.5-fold higher in MR and MR/GR cell lines (Fig. 1D).

We examined the cellular localization of the GR and MR by confocal microscopy, 6 h after incubation with either vehicle, dimethyl sulfoxide (DMSO) or 1 nM of the DEX. As expected, GR and MR proteins resided in the cytoplasm of untreated cells and translocated into the nucleus upon the addition of DEX (Fig. 1, *E–G*). Canonical GR target genes, FKBP5 and SGK1, were upregulated by DEX in GR and MR/GR cells but not in U-off or MR cells (Fig. S1). These genes were also upregulated by the selective MR ligand aldosterone in MR and MR/GR cells but not in U-off or GR cells. Consistent with previous reports (29, 38, 39), the level of gene induction mediated by activated MR was weaker than that mediated by
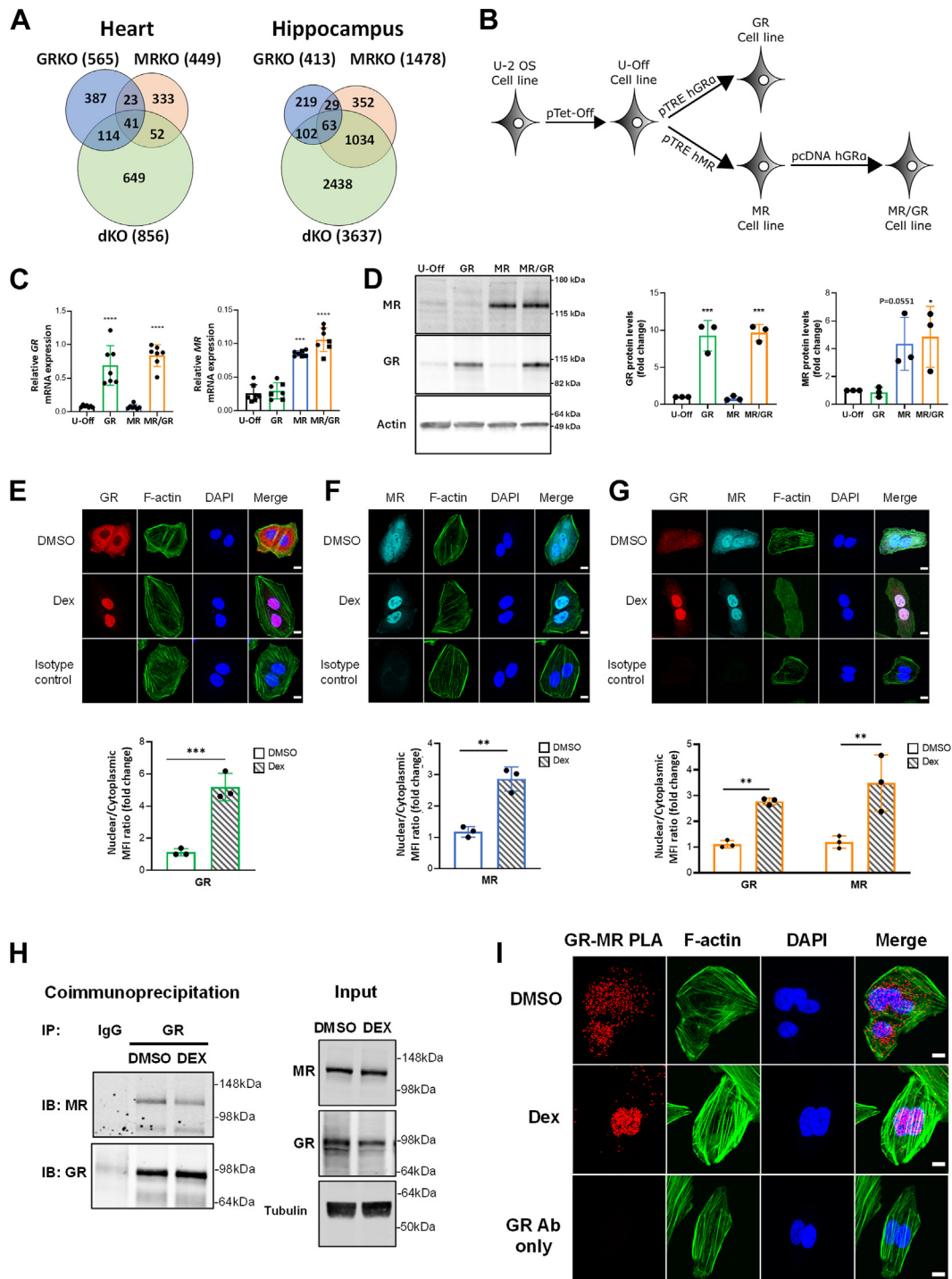
Figure 1. Establishing GR, MR, and MR/GR cell lines. *A*, Venn diagrams on heart and hippocampus gene expression change in GRKO, MRKO, and dKO mice compared to WT mice (32, 33). Much larger numbers of genes exhibited altered expressions in GR and MR double KO compared with GRKO or MRKO thus suggesting that the two receptors have functional interactions in these organs for the gene regulations. *B*, schematic diagram showing genealogy of cell lines used in this study. *C* and *D*, GR and MR mRNA (*C*) and protein (*D*) expression in the cell lines used in this study. Data are presented as means ± SD with individual data points of technical replicates. The data were analyzed using one-way ANOVA with Dunnett's *post hoc* test. *$p < 0.05$, ***$p < 0.001$, and ****$p < 0.0001$. *E*, *F*, and *G*, GR and MR protein localizations in the cell lines were determined by immunofluorescence histochemistry. The *upper panels* show the immunofluorescence histochemistry of receptors, and the *lower panels* show the quantifications of GR and MR localizations. *E*, GR protein localization in GR cells, (*F*) MR protein localization in MR cells, and (*G*) GR and MR protein localization in MR/GR cells before and after treatment with DEX (1 nM, 6 h). The scale bar represents 10 μm. Quantified data in (*E*), (*F*), and (*G*) are presented as mean ± SD with individual data points of technical replicates. The data were analyzed using Student's *t* test. **$p < 0.01$ and ***$p < 0.001$. *H*, coimmunoprecipitation of GR and MR protein extracted from MR/GR cells. *I*, proximity ligation assay (PLA) found GR and MR exist in close range in MR/GR cells. PLA signals in *red*, anti-F-actin staining in *green*, and nuclear staining with 4′,6-diamidino-2-phenylindole in *blue*. The scale bar represents 10 μm. ; DEX, dexamethasone; GR, glucocorticoid receptor; GRKO, GR knockout mice; MR, mineralocorticoid receptor; MRKO, MR knockout mice.

activated GR. These results demonstrate that we have established human cell lines that express functional GR, MR, or both GR and MR.

GR and MR interaction in MR/GR cell line

To investigate whether GR and MR are associated in a complex in MR/GR cells or not, we performed a coimmunoprecipitation assay and *in situ* proximity ligation assay (PLA) (40) as shown in Figure 1, *H* and *I*. In the MR/GR cell line, we found that MR coimmunoprecipitated with GR in the absence of ligands, and the complex formation persisted even upon 6-h treatment with DEX (Fig. 1*H*). We then performed a PLA to analyze MR and GR interaction. In untreated cells, the GR–MR interaction signals were detected within the cytoplasm as shown in red dots whereas, upon DEX exposure, fluorescent signals were observed within the nuclear compartment (Fig. 1*I*). These results indicate that GR and MR are associated in the same protein complex that can be detectable in the cytoplasm prior to DEX treatment and in the nucleus after the ligand induced GR and MR translocation.

RNA-seq analysis of DEX regulated genes in U-off, GR, MR, and MR/GR cells

To assess GR and MR interaction in gene regulation, we performed RNA-seq analyses on U-off, GR, MR, and MR/GR cells treated with 1 nM or 10 nM DEX for 6 h. Principal component analysis revealed little variation between untreated and DEX-treated U-off and MR cells. Conversely, we observed DEX-induced changes in gene expression in GR and MR/GR cells. However, the magnitude of the shift observed in GR cells was more pronounced compared to that in MR/GR cells (Fig. 2*A*). The gene expression analyses confirmed 6632, 114, and 1115 genes were differentially regulated by 1 nM DEX in GR, MR, and MR/GR cells, respectively (Fig. 2*B*). Similarly, with 10 nM DEX, we observed comparable changes in gene expression in GR, MR, and MR/GR cells, with 7291, 723, and 4776 genes being regulated, respectively. Only 1 and 106 DEGs (differentially regulated genes by DEX treatment) were found in the U-off cells by 1 nM and 10 nM DEX treatment, respectively. We excluded DEGs in U-off cells in the following discussion since this small number of DEGs did not affect our conclusions. The variation in the numbers of DEGs suggests that MR coexpression significantly mitigated the impact of DEX on gene expression in MR/GR cells compared to GR cells. Quantitative reverse transcription PCR was performed to validate the regulatory effects of DEX on gene expression for various genes identified from the list of DEGs in these three cell lines (Fig. S2). As shown in Figure 2*B* pie chart, in GR cells treated with both DEX concentrations, an almost equal number of genes were upregulated or downregulated. In contrast, disproportionally more genes were upregulated than downregulated in MR cells with 1 nM or 10 nM DEX. The asymmetric gene regulations caused by MR may also affect gene regulation in MR/GR cells which also showed a greater proportion of upregulated genes.

The Venn diagrams of DEGs in the cell lines are shown in Figure 2*C*. These diagrams revealed a substantial number of DEGs in GR cells (5627 and 3123 genes in 1 nM and 10 nM treated GR cells, respectively) were not responsive to DEX in MR/GR cells or MR cells. The majority of DEGs in MR cells are commonly regulated in GR cells and MR/GR cells. A small number of DEGs in the MR/GR cells (113 and 596 genes for 1 nM and 10 nM DEX, respectively) were regulated by DEX only when both receptors were coexpressed (Tables S1 and S2). These findings indicate that the major effect of MR coexpression is to limit the ability of GR to regulate target genes, rather than inducing expression of new target genes. We further analyzed the roles of MR in DEX-induced gene regulations in cells expressing both MR and GR. For this purpose, we compared genes regulated in GR cells and MR/GR cells in Venn diagrams (Fig. 2*D*). Almost 90% of DEGs in MR/GR cells are commonly regulated in GR cells (90% with 1 nM DEX and 87% with 10 nM DEX). In contrast, raising DEX concentration from 1 nM to 10 nM increased genes in the commonly regulated category from 15% to 57% of DEGs in GR cells. MR coexpression prevented 5630 genes and 3144 genes from responding to DEX at 1 nM and 10 nM concentrations, respectively. Furthermore, we compared induction levels of commonly regulated genes (1002 genes in 1 nM DEX-treated cells and 4147 genes in 10 nM treated cells) between these two cell lines (Fig. 2*D*, bottom panels). With both DEX concentrations, the commonly regulated genes showed reduced sensitivity to DEX treatment in MR/GR cells compared to those in GR cells as the slopes of the plots have much smaller value than 1 (0.5503 in 1 nM DEX-treated cells and 0.6929 in 10 nM DEX-treated cells). Overall, MR coexpression blunted DEX-GR–dependent gene regulations in both DEX concentrations.

We also compared GR cell *versus* MR cell as well as MR cell *versus* MR/GR cell (Fig. 2*E*). The first comparison revealed almost all MR-regulated DEGs were included in GR-regulated ones (99.1% of 1 nM and 94.3% of 10 nM regulated genes). Moreover, the commonly regulated DEGs responded to DEX less in MR cells compared with GR cells as indicated by the slope of each plot (slope for 1 nM DEX = 0.2427, for 10 nM DEX = 0.4444). For the MR cells *versus* MR/GR cells comparison, almost all MR-regulated DEGs are also regulated in MR/GR cells (96.5% of 1 nM and 91.7% of 10 nM DEGs in MR cells). Furthermore, responses of commonly regulated genes in MR/GR cells are higher than MR cells (slope for 1 nM DEX = 2.124, for 10 nM DEX = 1.19). These two comparisons indicated GR played dominant roles in DEX-induced gene expression modulations in these three cell lines. Thus, the comparisons in Figure 2, *D* and *E* revealed that MR has minor roles for DEX-induced gene expression by itself but plays remarkable roles in blunting the dominant GR effects on gene transcription and strongly implies the functional cooperation of these two receptors.

Gene expression profiling reveals that MR coexpression blunted GR-mediated alteration in pathways related to cell survival and apoptosis

Ingenuity pathway analysis (IPA; https://digitalinsights. qiagen.com/products-overview/discovery-insights-portfolio/ analysis-and-visualization/qiagen-ipa/) software was used to
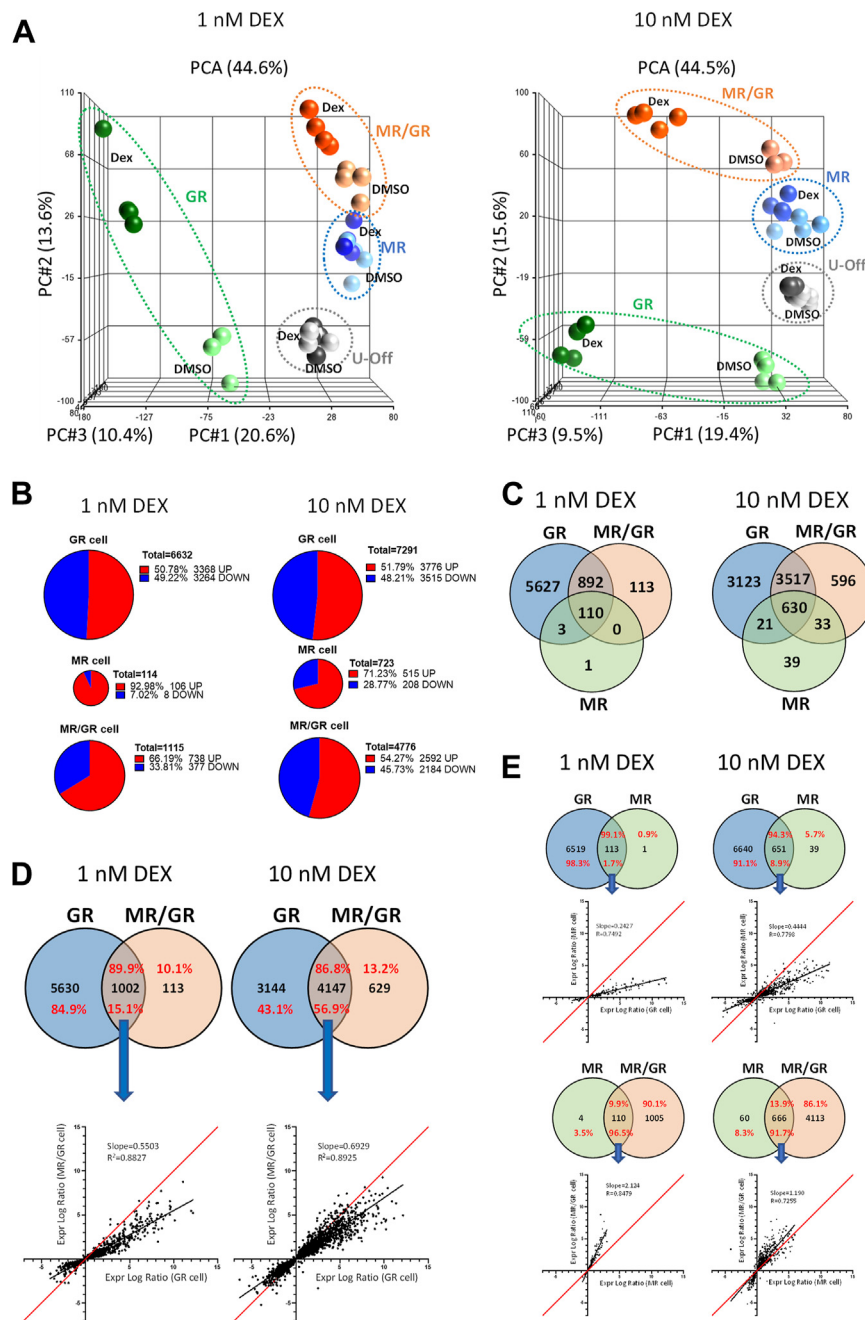
Figure 2. RNA-seq analysis of DEX-regulated genes in U-off, GR, MR and MR/GR cells U-off, MR, GR, and MR/GR cell lines were treated with 1 nM or 10 nM DEX and their gene expressions were measured by RNA-seq analysis. *A*, PCA results for U-off, MR, GR, and MR/GR cell lines treated with 1 nM DEX (*left panel*) or 10 nM DEX (*right panel*). *B*, induced (*red*) or suppressed (*blue*) gene numbers in GR, MR, and MR/GR cells treated with 1 nM or 10 nM DEX are shown in *pie charts*. *C*, Venn diagram for DEX-regulated genes in GR, MR, and MR/GR cells. *D*, MR blunted DEX-induced GR-mediated gene regulation. *Upper panels*: Venn diagram for DEX-regulated genes in GR and MR/GR cells. *Bottom panels*: Experimental log ratio of genes induced or suppressed commonly in GR cells and MR/GR cells were plotted. These plots suggested MR coexpression made gene induction or suppression less sensitive to 1 nM or 10 nM DEX treatments. *E*, as in Figure 3D, gene expression profiles were compared between two cell lines in Venn diagrams (*top*: GR cell *versus* MR cell, *bottom*: MR cell *versus* MR/GR cell). Experimental log ratios of commonly regulated genes were plotted in the same fashion as in Figure 3D and indicated genes in MR cells respond less compared to those in GR cells or MR/GR cells. DEX, dexamethasone; GR, glucocorticoid receptor; MR, mineralocorticoid receptor; PCA, principal component analysis.

uncover the molecular functional differences between GR cells and MR/GR cell's gene regulation responses to DEX treatment. Canonical pathway analyses are summarized in Figure 3A. We selected the top 20 canonical pathways based on absolute Z-scores in GR cells for further comparison among the three cell lines and treatments (1 nM and 10 nM DEX). IPA algorithm

calculates Z-scores to predict the activation state of the signaling pathway. These pathways were plotted in the order of −log10 (*p* value) with color-coded Z-scores and size-coded gene numbers. Overall, these plots indicated a strong blunting effect of MR coexpression on the signal pathways regulated by GR in response to DEX treatments.
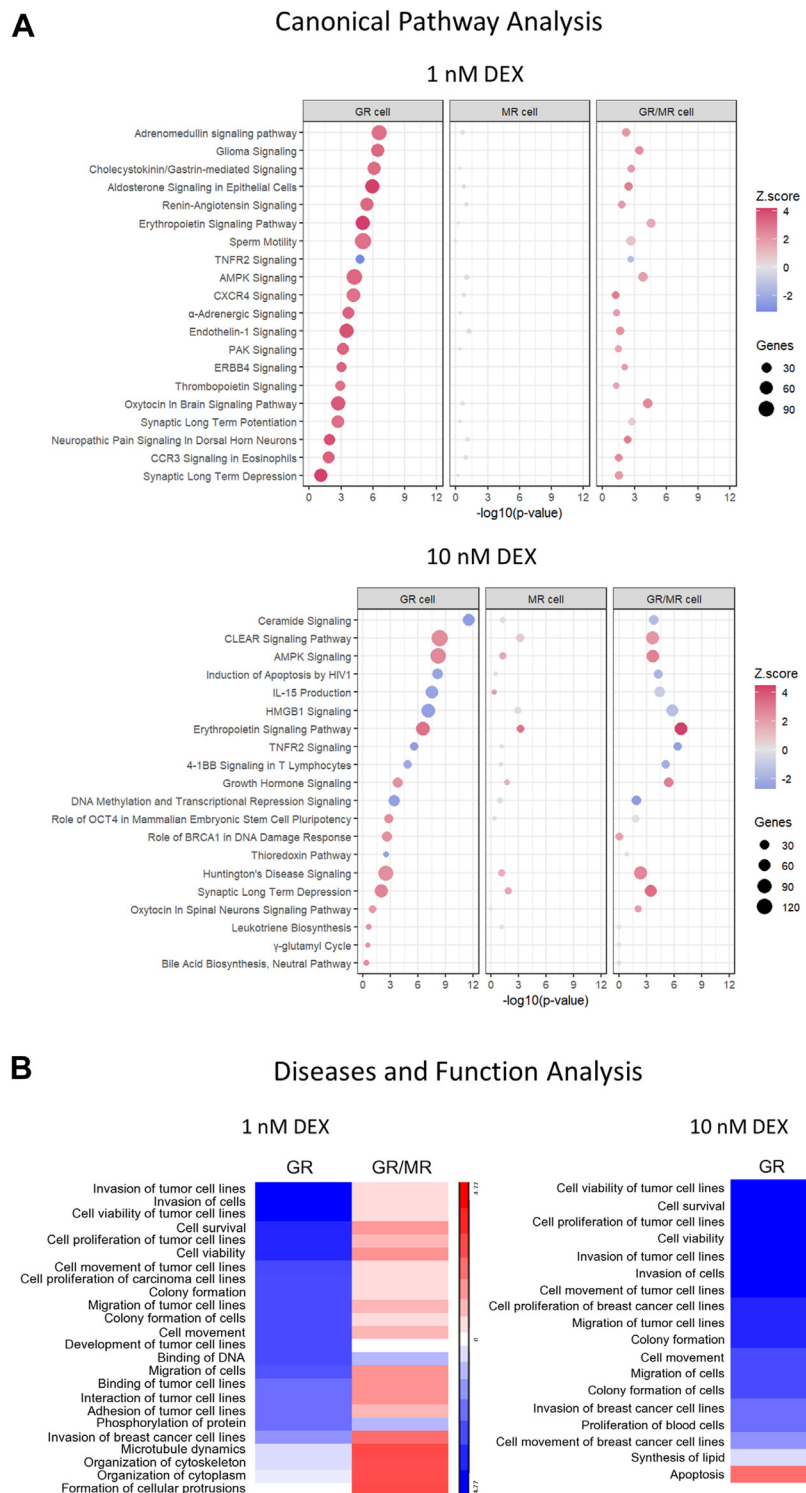
Figure 3. Pathway analyses of GR cell and MR/GR cell depicted blunting effect of MR coexpression. *A*, canonical pathway analysis results (1 nM DEX treatment for the *top panel* and 10 nM DEX treatment for the *bottom panel*) by ingenuity pathway analysis (IPA). Pathways which have the top 20 absolute Z-scores in GR cells were compared among GR, MR, and MR/GR cells. The pathways were plotted according to their −log10 (*p* value). *X*-axis represents −log10 (*p*value), circle size indicates number of genes, and color for the circle decodes for Z-score for each canonical pathway. *B*, comparisons of IPA diseases and function analysis between GR cell and MR/GR cell. Cellular functions with absolute Z-score bigger than 2 in either one of the two cell lines are shown as heat maps. DEX, dexamethasone; GR, glucocorticoid receptor; MR, mineralocorticoid receptor.

Diseases and function analysis also revealed similar MR coexpression effects for GR-mediated DEX-induced gene regulation. For visualizing Z-score differences in cellular functions, we made the comparison to annotations exhibiting Z-scores larger than 2.0 or smaller than −2.0 in either one of the two cell lines (Fig. 3*B*). Notably, these heat maps showed

that several common pathways have Z-score differences between these cell lines at both concentrations of DEX. For instance, pathways related to cell survival have lower Z-scores, and those related to cell death or apoptosis have higher scores in GR cells. Thus, these heat maps show that DEX induces more cell death and apoptosis in GR cells than in MR/GR cells.

MR coexpression suppresses DEX-induced apoptosis in GR cells, whereas MR knockdown restores DEX-induced apoptosis in MR/GR cells

Based on the IPA analysis, which indicated differential regulation of cell death and apoptosis by DEX in cells expressing GR and MR, we investigated the induction of apoptosis by DEX in GR and MR/GR cells. DEGs related to the apoptosis pathway in GR cells and MR/GR cells are presented in a heat map (Fig. 4A). Most of the DEX responsive genes in this category exhibited diminished responses in MR/GR cells compared to GR cells. We then examined DEX-induced apoptosis among GR, MR, and MR/GR cell lines after the cells were treated with vehicle (DMSO) or DEX (100 nM) for 48 h. We employed a higher concentration of DEX in this apoptosis assay than those in the gene regulation study in Figures 2 and 3 in order to observe clear biological effects and to be consistent with the DEX concentration used in previous reports evaluating glucocorticoid induced apoptosis in U2OS cells (36). DNA content was evaluated by propidium iodide (PI) staining and showed that, when treated with DEX,

Figure 4. MR coexpression suppresses DEX-induced apoptosis in GR-expressing cells. *A*, heat map showing diminished modulation of DEX-regulated genes related to apoptosis in MR/GR cells compared to those in GR cells. *B*, DEX induced cell death in GR cell, MR cell, MR/GR cell, and MR siRNA-treated MR/GR (MR/GR MR-KD) cells. MR coexpression suppressed the DEX-induced apoptosis in GR cells and apoptosis re-emerged when MR expression was suppressed. Cells were incubated with 100 nM DEX for 48 h. *C*, FACS quantification of cell death data shown in (*B*). *D*, MR mRNA and protein expressions in cell lines used for cell death analyses in (*B*). siRNA treatment of MR/GR cells (MR/GR MR-KD) effectively suppressed MR expression compared with control siRNA treatment (MR/GR NTC). *E*, propidium iodide negative and annexin-V positive cells quantification of cell lines treated with DEX as in (*B*) suggested cell death was caused by apoptotic mechanisms. *F*, PARP cleavage in the cells used in (*B*) double confirmed apoptosis is causing cell death observed in (*B*). Cleaved PARP and PARP amounts were determined by Western blotting as shown in the *right panel*. All quantified data in (*B*), (*D*), (*E*), and (*F*) are presented as mean ± SD with individual data points of technical replicates. The data were analyzed using one-way ANOVA with Sidak's *post hoc* test. *$p < 0.05$, ***$p < 0.001$, and ****$p < 0.0001$. DEX, dexamethasone; GR, glucocorticoid receptor; MR, mineralocorticoid receptor.

GR cells underwent 30% apoptosis. In marked contrast, neither MR nor MR/GR cells undergo apoptosis induced by DEX (Fig. 4, *B* and *C*). These results suggest that cell apoptosis induced by DEX-activated GR was suppressed by coexpression of MR. To determine whether MR knockdown can restore GR-mediated DEX-induced apoptosis in the MR/GR cells, we silenced MR expression by transfecting MR/GR cells with MR siRNA (MR/GR MR-knock down) (Fig. 4, *B* and *C*). Forty-eight hours posttransfection, MR mRNA level was reduced by 80% compared with MR/GR cells transfected with non-targeting control siRNA (MR/GR P), and MR protein knock-down was also observed (Fig. 4D). A variety of apoptotic endpoint assays including cell apoptosis (Fig. 4, *B* and *C*), externalization of phosphatidyl serine (Fig. 4E), and PARP cleavage (Fig. 4, *F* and *G*) after treatment with DEX for 48 h confirmed that the knockdown of MR in MR/GR cells restores the ability of liganded GR to induce apoptosis. These findings confirm that MR coexpression inhibits the GR-mediated apoptosis induced by DEX in MR/GR cells.

Nanobit assay revealed direct interaction of GR and MR in living cells

Our genomic and cell apoptosis analysis of the GR, MR, and MR/GR cells strongly indicated that GR and MR have functional interactions. To analyze the physical interaction of these two receptors in living cells, we have developed a method that can monitor GR–MR interaction in real time using "NanoBit" technology (41). This method uses two protein/peptide tags named "small tag" and "large tag" which are derived from one luciferase enzyme. When these two peptides are in close proximity, they can reconstitute the luciferase activity. As shown in Figure 5A, we have constructed a total of 8 fusion protein expression plasmids in which GR and MR have small tag or large tag at either their N-terminal or C-terminal side. We examined their reconstituted NanoBit luciferase activities by cotransfecting HEK293 cells with the GR and MR NanoBit fusion protein expression vectors (Fig. 5A). Luciferase activity is indicative of GR–MR interaction and this luciferase activity was induced by ligands only when GR and MR have these tags at the C-terminal ends. We evaluated the ligand effects of cortisol, DEX, and aldosterone (100 nM each) for the interaction using GR-LgTag + MR-SmTag expression plasmids (Fig. 5B). Our data show that the addition of the single ligand, cortisol, DEX, or aldosterone, induced these two receptors to interact almost immediately. Intriguingly, when DEX and aldosterone were added simultaneously, GR–MR interaction was enhanced synergistically compared with the single ligand effect. Similar GR–MR interaction profiles with lower luciferase activities were observed with 10 nM or 1 nM ligands (Fig. S3).

GR DNA binding null mutation interfered with DEX-induced GR homodimer formation, but not GR–MR heterodimer formation induced by DEX and aldosterone

One of the key factors for the homodimer formation of GR or MR is their DNA binding. Early studies employing gel shift assays have indicated that the DNA binding is essential for GR–MR interaction. They observed the complex including these receptors on short double strands of glucocorticoid response elements (20, 21). To examine the effect of GR DNA binding null mutations (Fig. 5, *C* and *D*) on GR homodimer (Fig. 5E) and GR–MR heterodimer (Fig. 5F) formation, we employed GR-LgTag and GR-SmTag expression vectors for GR homodimer Nanobit assay detection. We introduced previously reported GR DNA null mutations (42) into GR-SmTag expression vectors (C414Y, F444S, C463Y) completely abolished DEX-induced reporter gene activation in assays shown in Figure 5D. The same GR-SmTag mutants were used in GR homodimer (Fig. 5E) and GR–MR heterodimer (Fig. 5F) detection. These mutations effectively prevented the formation of GR homodimer. In contrast, GR–MR heterodimer formation was only marginally compromised by the same mutations. Thus, these differential effects on GR homodimer and GR–MR heterodimer highlighted critical differences in molecular mechanisms dictating homodimer and heterodimer formation.

Therapeutic glucocorticoids induced GR–MR heterodimers

Many therapeutic glucocorticoids targeting GR are currently prescribed for treating many types of diseases. To elucidate the specificity of ligand-dependent GR–MR heterodimer formation, we compared the effects of DEX, prednisolone, triamcinolone, and beclomethasone using NanoBit assay (Fig. 5G). Provocatively, all three of these drugs can induce GR–MR heterodimer formation, but they did so to markedly different degrees. We observed prednisolone with the strongest activity followed by beclomethasone showing almost the same activity with DEX and weak triamcinolone activity. We then examined the combination of the drugs with either aldosterone or cortisol (Fig. 5, *H–J*). As shown in Figure 5, *H* and *I*, beclomethasone or triamcinolone synergistically induced GR–MR heterodimerization with aldosterone. In contrast, cortisol moderately suppressed prednisolone heterodimer-inducing activity. These findings collectively suggest that glucocorticoid drugs have diverse potencies for inducing GR–MR heterodimers and corticosteroid in the body may differentially affect the potencies.

MR inhibits the ability of GR to interact with the genome

To investigate the GR cistrome in the presence or absence of MR, we performed chromatin immunoprecipitation sequencing (ChIP-seq) analyses using anti-GR antibody and DEX-treated GR and MR/GR cell extracts. We employed a higher concentration of DEX (100 nM) than RNA-seq study in Figures 2 and 3 to promote GR maximum occupancy on the genome since KD value of DEX to GR was 13.33 nM in GR cell (36). Marked reduction in the amount of GR bound on the genome (Fig. 6A) in MR/GR cell compared to GR cell. The Venn diagram shown in Figure 6B summarizes the number of peaks observed for these cells and their relations. More than 32,000 peaks were observed for GR cells, whereas less than 7600 peaks were found for MR/GR cells, revealing a major inhibitory effect by MR on GR binding to the genome. Among
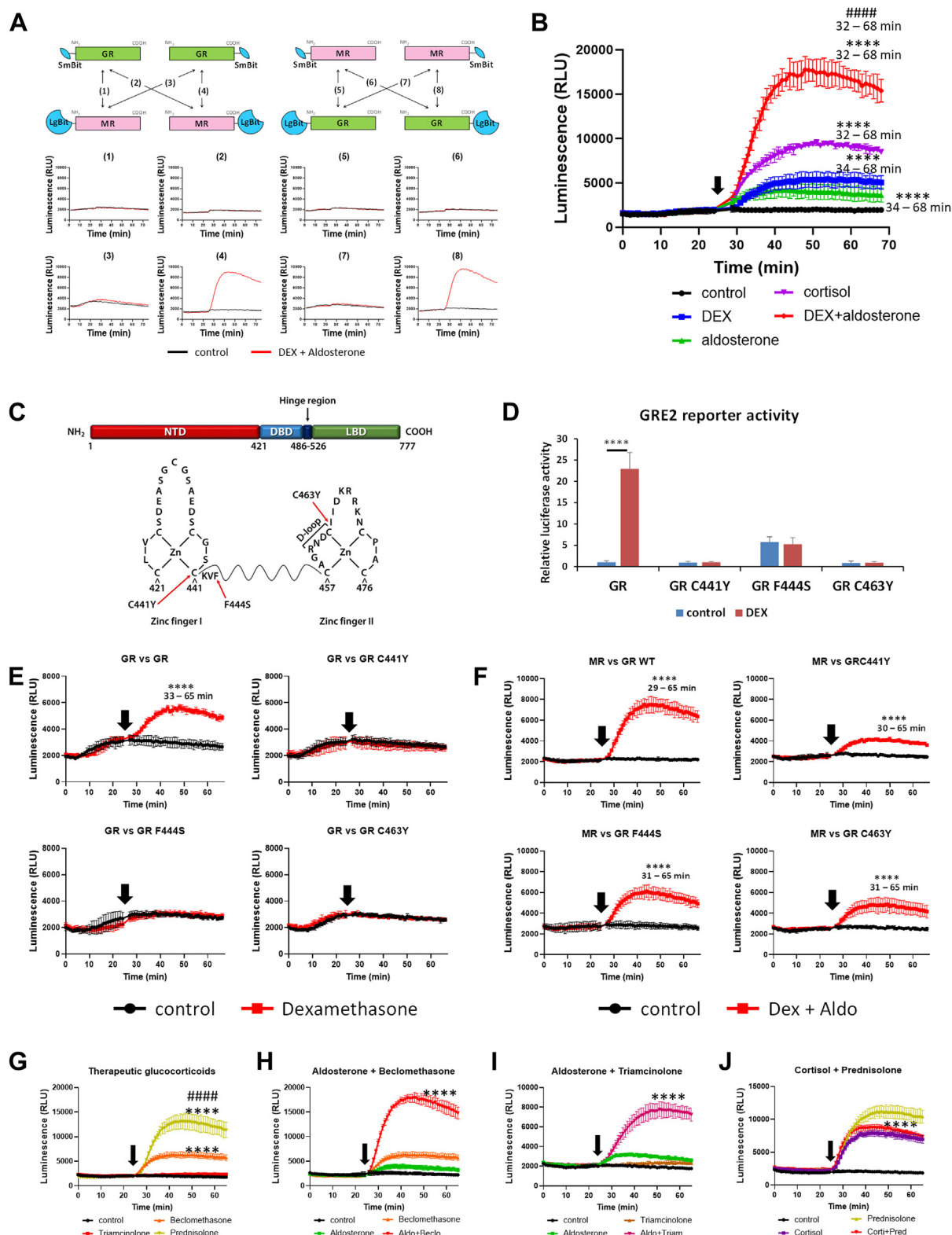
Figure 5. NanoBit assay revealed direct interaction of GR and MR in living cells. *A*, in combination of GR and MR with Nanobit luciferase derived fragments (LgBit and SmBit), total of 8 constructs were produced. All combinations (1–8) were examined for reconstituted NanoBit luciferase activity. Only two of them with the luciferase fragments existing at the C-terminal side of the receptors (4, 8) showed robust luciferase activity by the additions of ligands (DEX and aldosterone) at 25 min after starting the measurement of the luciferase activity. *B*, single ligand (DEX, aldosterone, or cortisol, 100 nM) induced GR–MR interaction, and further heterodimerization was observed by DEX and aldosterone added simultaneously. Data are presented as mean ± SD. The data were analyzed using two-way ANOVA with Tukey's *post hoc* test. Each treatment group showed significant induction of Nanoluc luciferase activity compared to activities in control (****$p < 0.0001$ at shown time periods). DEX + aldosterone-induced activity was higher compared to those in DEX or aldosterone single ligand treatments (####$p < 0.0001$ 31–68 min). *C–F*, zinc finger mutations affect differentially GR–MR heterodimerization and GR–GR homodimerization. *C*, GR zinc finger DNA-binding domain and three critical amino acid mutations for DNA binding (42). *D*, GRE2 reporter gene

these, 25,650 peaks were specific to GR cells, 6761 peaks were common, and 816 peaks were specific to MR/GR cells. Heat map presentation showing the size distribution of the peaks in each specific group are presented in Figure 6C and no differences were observed among the cell lines. Examples of genes that gave unique peaks for GR cells (KCNA5) and a common peak (KLF5) in both GR and MR/GR cells are presented in Figure 6D. mRNA for KCNA5 and KLF15 was quantified by qPCR in Figure 6E. Consistent with ChIP-seq data, KCNA5 was induced only in GR cells by DEX, and KLF15 was induced in GR cells and showed only a trend for DEX regulation in MR/GR cells. Additional data for validating MR-suppressed GR interaction with genome are presented in Fig. S4.

Molecular dynamics simulation of GR–MR LBD heterodimer

In a previous report, 4 GR-LBD and MR–LBD heterodimer model structures were suggested based on available GR or MR homodimer structures found in crystal 3D analyses (30). However, we found only one of them based on reported MR crystal structure (37) is permissive with our NanoBit assay results in Figure 5. In this LBD configuration, C-terminal ends of the GR and MR LBDs are located close enough for NanoBit luciferase activity reconstitution. Therefore, we employed this model structure of GR/MR heterodimer as the starting structure of three independent molecular dynamics (MD) simulations (Fig. 7A).

The RMSDs calculated for each monomer exhibit fairly stable monomer conformations for all three trajectories (Fig. 7B). In two trajectories, dimer conformations remained relatively close to the starting model while in the third trajectory, the two monomers adopted a slightly shifted orientation. The RMS fluctuations calculation suggested GR shows higher fluctuations (Fig. 7C) in the residue regions of 540 to 560, 620 to 640, and around 680, 740 to 750. Meanwhile, the residue segment 700 to 728 is a loop and a part of a helix. The mobility here may be somewhat associated with the interfacial rearrangement due to protein–protein interactions. This region is in contact with the C-terminal region of MR which is highly mobile, likely due to the truncation in the simulated system. In MR molecule, the regions around residues 760 and 840 are in loop structures, and the large peak around residue 910 is due to the reconstruction of the missing loop in the X-ray crystal structure. The consorted motions of various segments are captured through the dynamic cross correlations shown in Figure 7D. The blue regions represent the consorted motion while the other regions are more random in terms of

their relative motion. Specifically, in the highlighted areas through vertical and horizontal lines in Figure 7E, one can observe the conserved motion in segments of GR and MR. Our MD simulation results indicated that GR-LBD and MR-LBD contribute stable heterodimer formation between GR and MR molecules through the interfaced shown in Figure 7A. Based on these model structures, we obtained free energy values of each residue for the LBD heterodimer stabilization as summarized in Figure 7F and Fig. S4.

We mutated Trp 712 to Ala in GR, one of the residues with a high free energy contribution for the LBD heterodimer stabilization in our simulation as shown in Figure 7F, then performed NanoBit analysis (Fig. 7, G–J). This single mutation compromised GR–MR interaction in the assay and the reconstituted luciferase activity by MR and GR W712A was 32% of that produced by WT receptors. This observation strongly supports the existence of the proposed LBD heterodimer model structure. In contrast, the same mutation did not attenuate GR homodimer formation (Fig. 7, I and J). Consistently, glucocorticoid response element (GRE) luciferase gene reporter shows that activation by GR was not affected by W712A mutation (Fig. 7I).

Discussion

Although mineralocorticoid and glucocorticoid are adrenal steroid hormones that have completely different physiological activities, their receptors, GR and MR, are highly homologous and bind to identical DNA regulatory elements (43, 44). Ligand-dependent activation of these receptors drives both to form homodimers and to bind to DNA response elements on target genes. Because of their high homology and because each receptor forms a homodimer, it has also been hypothesized that GR–MR forms a heterodimer which was indeed found *in vitro* or cell line systems (20–24, 45). These earlier studies were based on *in vitro* complex formation with DNA elements in gel shift and gene reporter assays. However, clear physiological functions for GR–MR heterodimer remain undefined, and GR–MR interactions at the molecular level are poorly understood.

Our recent results using gene KO mice provocatively suggested GR–MR functional interaction in the heart and hippocampus (32–34). These observations urged us to focus on GR–MR interaction at the molecular level since such information could become a base for elucidating mechanisms behind the observed functional interactions of the receptors in mice. Furthermore, this information will be critically important for designing new ligands with distinct functions for disrupting the

---

activation by WT GR or the three mutants shown in (C). Data are presented as mean ± SD. The data were analyzed using two-way ANOVA with Sidak's *post hoc* test. ****$p < 0.0001$. E, the three mutants compromised GR–GR homodimerization activity. Data are presented as mean ± SD. The data were analyzed using two-way ANOVA with Sidak's *post hoc* test. (****$p < 0.0001$). F, compared to WT GR, three zinc finger mutants retained partial heterodimerization activity with MR. Data are presented as mean ± SD. The data were analyzed using two-way ANOVA with Sidak's *post hoc* test. (****$p < 0.0001$). G–J, therapeutic glucocorticoids induced GR–MR heterodimer. G, beclomethasone and prednisolone but not triamcinolone induced GR–MR heterodimer formation. Each drug was added (final concentration 100 nM) into the culture media and monitored Nanoluc luciferase activity time course changes. Data are presented as mean ± SD. The data were analyzed using two-way ANOVA with Tukey's *post hoc* test. (****$p < 0.0001$ 29–65 min compared to control. ####$p < 0.0001$ significant difference between beclomethasone and prednisolone during 31–65 min time points). H and I, aldosterone (100 nM) cotreatments with beclomethasone (100 nM, panel H) or triamcinolone (100 nM, panel I) synergistically induced GR–MR heterodimer. Data are presented as mean ± SD. The data were analyzed using two-way ANOVA with Tukey's *post hoc* test. ****$p < 0.0001$ between double ligands and each ligand. J, cortisol (100 nM) partially suppressed prednisolone (100 nM) induced heterodimer formation. Data are presented as mean ± SD. The data were analyzed using two-way ANOVA with Tukey's *post hoc* test. ****$p < 0.0001$ between cortisol and cortisol + prednisolone treatments during 36 to 65 min. DEX, dexamethasone; GR, glucocorticoid receptor; MR, mineralocorticoid receptor.
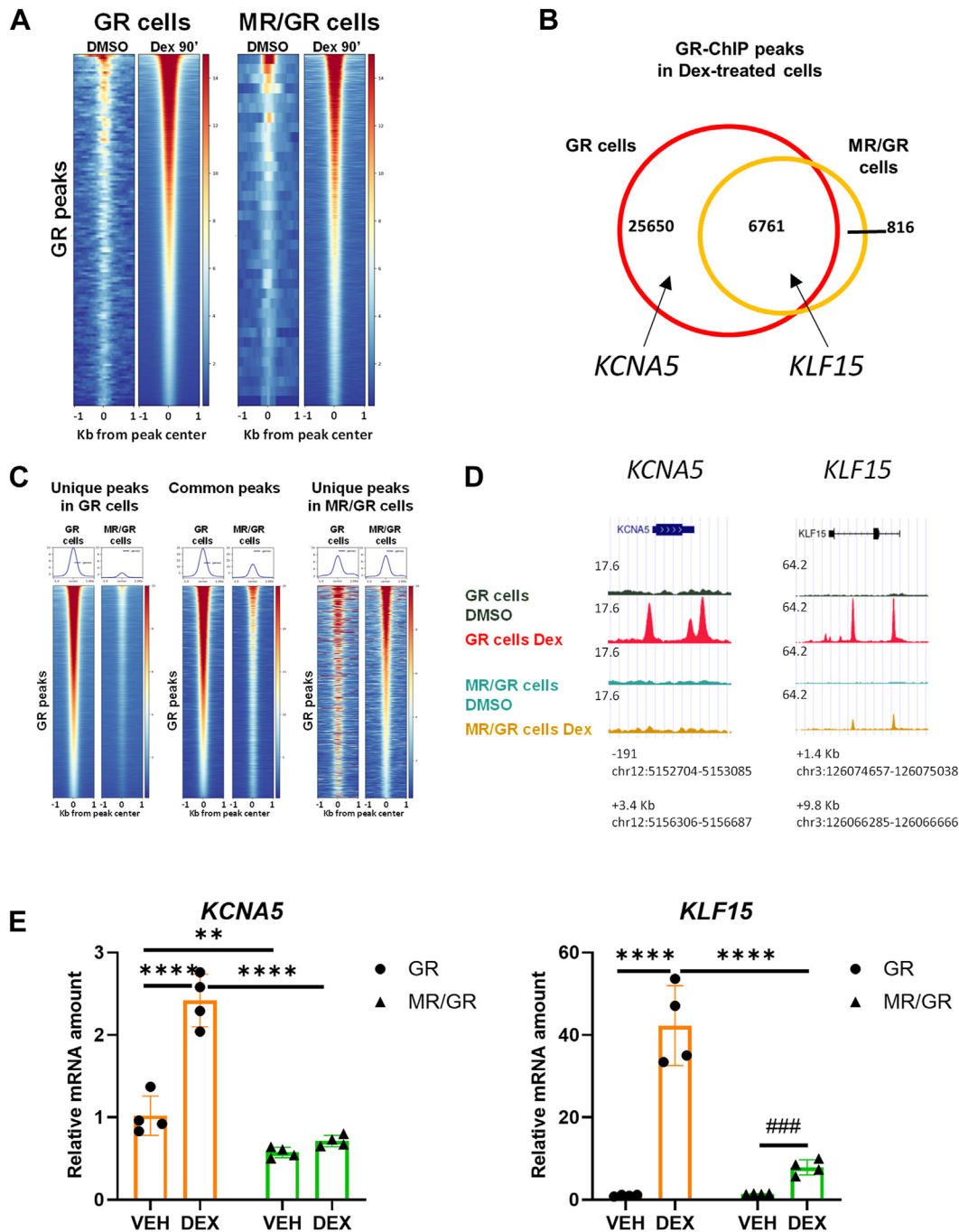
Figure 6. MR-suppressed GR interaction with genome in MR/GR cells. *A–D*, ChIP-seq analysis revealed attenuated GR binding to DNA elements by MR coexpression. *A*, heat map presentation of GR binding to DNA elements in GR cells and MR/GR cells. *B*, Venn diagram showing overlapping GR binding peaks of MR cells and MR/GR cells found in ChIP-seq analysis. MR coexpression suppressed GR binding to the genome. *C*, heat map presentation of the GR binding peaks categorized by Venn diagram shown in (*B*). *D*, examples of ChIP-seq identified peaks in *KCNA5* and *KLF15* genes that are in the "unique" and "common" peaks category, respectively. Locations of identified GR binding sites in chromosomes for these genes are shown at the *bottom*. *E*, qPCR quantification of *KCNA5* and *KLF15* mRNA in GR cell and MR/GR cell with or without DEX (100 nM, 6 h) treatment. Data are presented as mean ± SD with individual data points of technical replicates. The data were analyzed using two-way ANOVA with uncorrected Fisher's least significant difference post *hoc* test. **$p < 0.01$, ****$p < 0.0001$. ###In MR/GR cell, DEX induction of *KLF15* gene was nonsignificant by two-way ANOVA (0.0898). Student's *t* test suggested $p = 0.00412$. ChIP-seq, chromatin immpunoprecipitation sequencing; DEX, dexamethasone; GR, glucocorticoid receptor; MR, mineralocorticoid receptor.

interaction of these two receptors. Thus, in this study, we have developed experimental cell systems for analyzing specifically gene regulation and biological functions attributed to the GR–MR interaction. To this end, we generated GR cells, MR cells, and MR/GR cells from human U2-OS cells, which have negligible expression of GR and MR. We compared responses

to DEX treatment by analyzing changes in gene expression to assess the functional interaction of GR and MR.

The extensive genomics data about the transcriptome of GR cell and MR/GR cell revealed that MR functioned predominantly to limit the GR response to DEX. GR alone was hyperreactive to the glucocorticoid and regulated over 6600
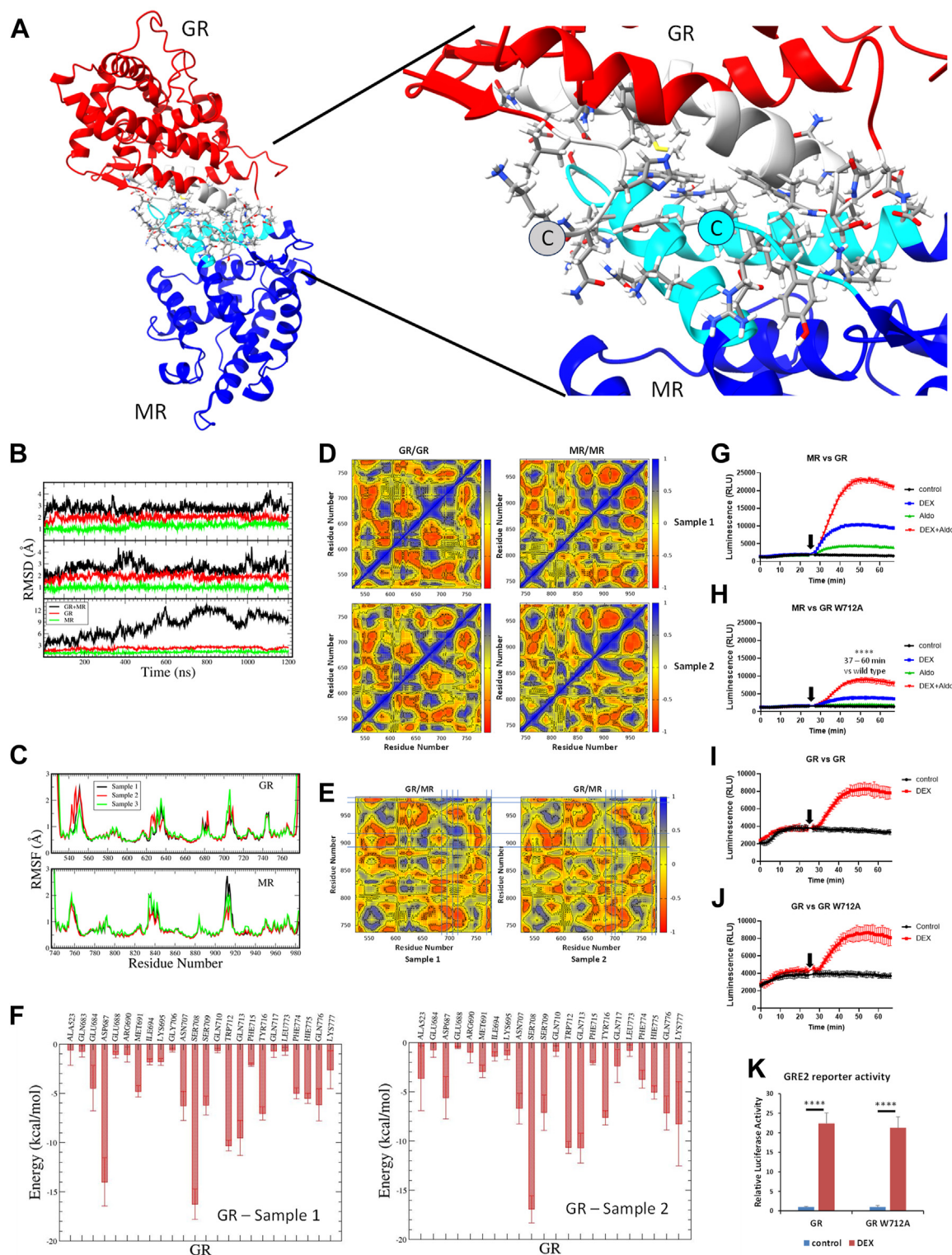
Figure 7. Molecular dynamics simulation of GR–MR LBD heterodimer. *A*, a representative solution structure of GR/MR heterodimer. GR residues are shown in *red and white ribbons* and MR in *blue and cyan*. Dimer-interacting surfaces of GR and MR are comprised of *white and cyan ribbons* and it involves the C termini of GR and MR marked in the *circles* with "C" inside. *B*, RMSDs of GR (*red*), MR (*green*), and the GR/MR dimer (*black*) from the three independent molecular dynamics simulations of 1.2 μs each. The trajectory represented in the *bottom panel* shows an unstable GR/MR heterodimer interface. *C*, residue RMS fluctuations of the backbone heavy atoms for each residue of GR (*top*) and MR (*bottom*) from the two molecular dynamics trajectories (*red and green*) with stable dimer interface. *D*, dynamic cross correlation matrices of GR and MR monomers. *E*, GR/MR dynamic cross correlations. Interacting residue ranges are marked. *F*, interaction energies decomposed at the residue level for GR residues using MMGBSA calculations. Labels "Sample 1" and Sample 2" are energies from the two trajectories with stable dimer interacting interfaces. Averages and error bars were calculated from the 1200 sample points collected over each trajectory. *G* and *H*, GR Trp 712 mutation attenuated GR–MR interaction in NanoBit assay. MR and WT GR (*G*) or MR and GR W712A (*H*) interaction was analyzed by NanoBit assay. Data from one 96-well plate assay were shown in two panels. Data are presented as mean ± SD. The data were analyzed

genes with only 1 nM DEX stimulus. The coexistence of MR mitigated this hyperreactivity and limited regulated genes to around 1100. More than 83% of genes reactive to DEX were not responsive when MR was present with GR in the cell. Consistently, cistrome analysis revealed GR bindings on the genome were inhibited by the presence of MR (Fig. 6). The canonical pathway analysis of the genomics data indicates that the MR inhibited DEX-modulated pathways selectively (Fig. 3*A*). For example, with 1 nM DEX treatment, MR coexpression effects on "erythropoietin signaling pathway," "AMPK signaling," and "oxytocin in brain signaling pathway" were modest compared with the other DEX-modulated pathways such as the "adrenomedullin signaling pathway" and "renin-angiotensin signaling." Such MR selective effects on pathways were also observed in 10 nM DEX-treated cells (Fig. 3*A*). Activation Z-scores found in "diseases and function analysis" in Figure 3*B* revealed the scores for most pathways were changed from negative to positive in 1 nM DEX-treated cells, suggesting these pathways were inhibited by glucocorticoids in GR cells but activated in GR/MR cells. Therefore, the MR appears to globally repress GR transcription factor activity in order to specifically direct cell biological responses.

One of the major biological responses predicted by IPA to be inhibited by MR coexpression with GR was apoptosis (Fig. 3). Indeed, we observed that GR-dependent DEX-induced cell apoptosis was attenuated in GR/MR cells and this effect was reversed by knockdown of MR (Fig. 4). This result is consistent with a previous report showing that overexpression of the N-terminal domain (1–516) of MR blocked glucocorticoid induced apoptosis in a human B lymphoma-derived cell line (46). Our study builds on this prior work by showing that the inhibitory activity of MR on GR-mediated cell death occurs with the full-length MR, in a different human cell type (osteosarcoma cells), and in response to a different glucocorticoid ligand (DEX). Moreover, our study captures the global gene changes associated with apoptosis that are altered by the presence of MR in the DEX-treated GR/MR cells. Notably, 10 of the 11 genes whose regulation by GR was suppressed by MR in quantitative PCR (qPCR) validation studies of our RNA-seq findings have roles in apoptosis (Fig. S2). Since glucocorticoids are known to induce the killing of some cell types (thymocytes, osteoblasts) but promote the survival of others (hepatocytes, cardiomyocytes) (47), our data suggest the level of MR coexpression may contribute to the sensitivity of cells to glucocorticoid-induced apoptosis. Taken together, our results suggest that the ability of MR to interact with GR modulates the genetic and biological activity of GR to control cellular responsiveness to glucocorticoids.

The molecular mechanisms responsible for the reduced GR binding to the genome in the GR/MR cells are currently unknown and remain to be elucidated in future studies. GR/MR heterodimers may have reduced affinity for the genome and/or be less stable once bound compared to GR/GR homodimers. Protein factors including nuclear receptor coregulators that can specifically interact with GR–MR heterodimer may play critical roles modulating its DNA binding profile (11, 12, 48–51). This unidentified mechanism implies GR activity being regulated by MR in a tissue-specific manner since it is dependent on the concentration of MR. Our findings in this report are based on the model cell line system, and the GR–MR interaction may give different responses in other cell types. Thus, it remains to be tested whether similar MR blunting effects on GR-mediated gene regulations play any roles in the GR–MR functional interactions we discovered in mouse heart and hippocampus (Fig. 1*A*).

We employed NanoBit technology for monitoring GR–MR interaction in living cells after the addition of ligands (Fig. 5). Since this method detects reconstituted luciferase enzyme activity produced by two peptides called large-bit and small-bit derived from NanoBit luciferase, positive activity detection indicates the direct interactions of the peptides. Thus, the attaching points in your target proteins (usually at N terminus or C terminus of the proteins) must be at a very close distance and strongly suggest direct interactions of the two partner proteins. Furthermore, the luciferase activity can be monitored in living cells in real-time and thus we can trace protein interaction and dissociation in a time-course manner. Indeed, time course changes of detected luciferase activity showed that the interaction between GR and MR occurred within a few minutes after the addition of ligands and persisted throughout the treatment (Fig. 5). Intriguingly, not only therapeutic glucocorticoids (prednisolone and beclomethasone) by themselves but also combinations of the drugs (beclomethasone and triamcinolone) with aldosterone show strong inductions of the heterodimer formation (Fig. 5, *G–J*). The heterodimer inductions by these three drugs provide a possible underlying mechanism of unexpected side effects caused by the drugs in this class and the analyses of the detail of differential heterodimer induction by the drugs may be an exploitable target for fine-tuning glucocorticoid drug treatments.

In the last several years, groups have reported GR and MR functional and gene regulatory cooperation in multiple tissues and cell types. However, none of these results showed MR-suppressing effect on GR-dependent gene regulations. For example, in keratinocytes, GR and MR cooperatively regulate epidermal development and suppress skin inflammation (27). The number of GR binding sequences by ChIP-seq analysis on immortalized MR knockout mice keratinocytes was reduced by 35% (31) contrasting to our results showing MR coexpression decreased GR binding to GRE in GR/MR cells (Fig. 6). Moreover, the presence or absence of MR in the keratinocytes had only minor impacts on the DEX transcriptome. Other groups also reported GR–MR coactivation of target genes

---

using two-way ANOVA with Tukey's *post hoc* test. (****$p < 0.0001$ during 30–67 min between the luciferase activities of MR interactions with WT or W712A with the same ligand treatment). *I* and *H*, GR Trp 712 mutation did not affect GR–GR interaction in NanoBit assay. WT GR-SmBit and WT GR-LgBit (*I*) or WT GR-SmBit and GR W712A-LgBit (*J*) interaction was analyzed by NanoBit assay. *K*, Trp 712 mutation to Ala did not affect GR activity for GRE2 luciferase reporter gene. Data are presented as mean ± SD. The data were analyzed using one-way ANOVA with Sidak's *post hoc* test. ****$p < 0.0001$. GR, glucocorticoid receptor; LBD, ligand-binding domain; MR, mineralocorticoid receptor.

![ASBMB]

J. Biol. Chem. (2025) 301(5) 108488 **13**

based on genome wide studies on rat hippocampus (25) and N2A mouse neuroblastoma cells (29) or PER1 gene study in a renal cell line expressing GFP-hGR (28). Collectively, these findings suggest there is cell-type specificity in the gene regulatory and functional profiles of GR–MR heterodimers that may depend on the relative expression level of these two receptors in different cells and tissues. We observed strong Nanoluc luciferase activity when we used GR and MR with C-terminal NanoBit tag peptides (Fig. 5). Using available crystal structures of these receptors and Protein Interaction by Structural Matching tool, four configurations of the heterodimer have been proposed (30). Among four configurations, only one allows C-terminal tag direct interaction for the luciferase activity reconstitution. The configuration that gives close C-terminal ends was based on MR LBD homodimer crystal structure (37) and we utilized this configuration as the starting structure for MD simulation. The results indicated that GR and MR LBD interaction in this configuration is sufficiently stable. Furthermore, contributing amino acids for energy stabilization localized on helix 9, 10, and 11 plus a short segment near the C-terminal of these receptors were identified (Figs. 7, S4). None of these regions are known to be involved in direct ligand interactions. We mutated Trp 712, one of such amino acids in helix 10, and found the W712A mutant effectively compromised the GR–MR interaction (Fig. 7, *G* and *H*). Since Trp 712 is one of the amino acid residues with substantial energy contribution to our model GR–MR heterodimer (Fig. 7*F*), the results strongly support our proposed LBD heterodimer formed in the cells. By contrast, transcriptional activation of GRE reporter was not affected at all by the same mutation in GR molecule (Fig. 7*I*) suggesting that GR potency as a transcriptional activator and its ability to form the heterodimer with MR are functionally independent. A similar conclusion was implied by our DNA binding null GR mutants shown in Figure 5, *C–F*. Although the three mutants have no transactivation activity or the ability to form GR homodimers, they formed heterodimers with MR. Thus, GR's ability to form a homodimer for target gene activation is independent of its ability to form heterodimers with MR.

Overall, our findings provide strong evidence for a new nuclear receptor signaling paradigm where heterodimers of distinct nuclear receptors elicit genetic and biological signatures that differ from their respective homodimers. In the case of GR, its interaction with MR may contribute not only to the diverse actions of glucocorticoids but also to the development of tissue-specific glucocorticoid resistance and the adverse effects that arise from chronic glucocorticoid therapy. Genomics data in this article provides a reference for future analyses for defining GR–MR interaction in mammalian biology and is pivotal information for elucidating context-dependent GR activation mechanisms. Our NanoBit detections of GR and MR interactions will give us a powerful tool for detecting natural and synthetic ligands capable of inducing two receptor interactions. Furthermore, with the information on interacting amino acid residues in our model structure, the assay may be used to establish mutants completely lacking the interaction but retaining their activities as transcription factors for

defining biological functions of such receptor interactions. Thus, overall, the data in this paper revealed unknown molecular functions and gene regulation mediated by GR–MR interactions and will contribute to defining such molecular interaction in signaling mechanisms of these medically important nuclear receptors in both health and disease.

Experimental procedures

Cell lines and their culture

The U-off cell line and GR cell were established as in a previous publication (52). To generate the MR cells, the coding region of human mineralocorticoid receptor was cloned into pTRE2hyg vector and transfected into the U-off cells, and stably expressing clonal populations were selected using 500 μg/ml of Geneticin and 500 μg/ml of hygromycin. One clonal MR cell was chosen for transfection with pcDNA-hGR and selected using 500 μg/ml Geneticin, 500 μg/ml hygromycin, and 1 mg/ml Zeocin to generate a cell line expressing both GR and MR (MR/GR cell). The human U-2 OS stable cell lines, U-off, GR, MR, and MR/GR cells were maintained in Dulbecco's modified Eagle's medium/F-12 supplemented with 10% fetal calf serum and appropriate antibiotics (200 μg/ml Geneticin, 200 μg/ml hygromycin, and 400 μg/ml Zeocin). HEK-293 (American Type Culture Collection) cells were cultured in minimum essential media supplemented with 10% fetal bovine serum. Cell cultures were tested for *mycoplasma* according to previously published methods (53). All cell lines used in this study were authenticated using short tandem repeat profiling.

RNA isolation and quantitative reverse transcription PCR

Total RNA was isolated using the RNeasy mini kit (Qiagen) and 100 ng of total RNA were used to perform the one-step quantitative real-time PCR using iTaq Universal Probes One-Step Kit (Bio-Rad). Expression of mRNAs was normalized to PPIB gene using the relative expression or ΔΔCt methods. Real time qPCRs were performed using the CFX96 detection system (Bio-Rad). The TaqMan real time PCR assay probes (Thermo Fisher Scientific) are listed in Table S3.

RNA-seq analysis

All RNA-seq libraries (nonstrand-specific, paired-end) were prepared with the TruSeq RNA Sample Prep kit (Illumina). Poly(A) enrichment was conducted on the total RNA samples as outlined in the TruSeq protocol. The resulting mRNA samples were sequenced utilizing the paired-end 75 bp protocol on either the NextSeq 500 or NovaSeq 6000 platform from Illumina, following the manufacturer's guidelines.

The raw reads underwent filtering based on a mean base quality score exceeding 20, and adapter trimming was executed using "Trim Galore" (version 0.4). The trimmed reads were aligned to the hg19 reference genome using STAR aligner (version 2.6) (54). Gene quantification was conducted using Subread featureCounts (version 1.4.6) (55) eight utilizing the UCSC hg19 RefSeq gene release (downloaded August 18th, 2017) as the reference. The quantification outcomes from featureCounts were subsequently subjected to analysis *via* the

Bioconductor package DESeq2 (https://bioconductor.org/packages/release/bioc/html/DESeq2.html) (56), which fits a negative binomial distribution to estimate technical and biological variability.

Comparisons between the vehicle and treatment samples were conducted to detect differentially expressed genes. To adjust the false discovery rate (FDR), the Benjamini and Hochberg method was employed. A gene was deemed significantly differentially expressed if the FDR-adjusted p value for differential expression was below 0.05.

Pathway analysis

The significant genes underwent pathway and network analysis using the IPA tool (version 44691306) from Ingenuity Systems, based in Redwood City, CA.

Western blotting

Proteins were separated on Tris-glycine gels (Thermo Fisher Scientific) and transferred to nitrocellulose membranes. Target proteins were detected with anti GR (clone D8H2, Cell Signaling Technology, 1:1000), anti-MR (clone ID5 from Dr Celso Gomez-Sanchez, 1:500) (57), anti-actin (clone C4, MilliporeSigma, 1:10,000), anti-tubulin (clone DM1A, MilliporeSigma, 1:10,000), and anti-PARP(Cell Signaling Technologies, 1:1000). Anti-GR and anti-MR specificities were validated in the previous publication (33). The secondary antibodies used were IRDye 800CW goat anti-mouse IgG (LI-COR Biosciences), and Alexa Fluor 680 goat anti-rabbit IgG (Thermo Fisher Scientific). Signals were quantified using the LI-COR Odyssey imaging system (LI-COR Biosciences).

Immunoprecipitation assay

GR–MR protein complex immunoprecipitation assays were performed as in the previous report (56). Cell lysates were incubated overnight at 4 °C with anti-GR (clone D8H2, Cell Signaling Technology), or rabbit IgG antibody (MilliporeSigma). Immunocomplex was precipitated with protein A/G agarose (Thermo Fisher Scientific) and analyzed by Western blotting analysis using anti-GR or anti-MR antibodies.

Immunofluorescence stainin and in situ PLA

Cells grown in Nunc lab-tek chamber slides (Thermo Fisher Scientific) were fixed with 4% paraformaldehyde for 20 min at room temperature and blocked with PBS containing 5% normal goat serum, and, 0.1% Triton-X-100 at room temperature for 1 h. The cell samples were incubated with rabbit anti-GR (clone D8H2, Cell Signaling technology 1:100) or anti-MR (clone ID5 from Gomez-Sanchez, 1:50) for overnight at 4 °C. Anti-GR and anti-MR specificities for immunofluorescence staining were validated in the previous publication (33). The samples were then washed with 1X PBS containing 0.1% Tween, and incubated with Alexa Fluor 488 phalloidin (Thermo Fisher Scientific, 1:100), and the secondary antibodies goat anti-rabbit Alexa Fluor 594, goat anti-mouse Alexa Fluor 594, or goat anti-mouse Alexa Fluor 647 ((Thermo Fisher Scientific, 1:500) for 1 h at room temperature. Samples

were mounted with ProLong gold antifade with 4′,6-diamidino-2-phenylindole (Thermo Fisher Scientific). A Zeiss laser scanning confocal microscope (LSM 880; Carl Zeiss) was used to analyze GR and MR cellular distribution.

In situ PLA detection of GR and MR interaction was performed using Duolink PLA kits (Duolink In Situ PLA Probe Anti-Rabbit PLUS and Duolink In Situ PLA Probe Anti-Mouse MINUS, MilliporeSigma) according to the manufacturer's instructions. MR/GR cells were grown in 35 mm glass-bottom microwell culture dishes (MatTek corporation). Antibodies used were rabbit anti-GR antibody (clone D8H2, Cell Signaling technology 1:1000) and mouse anti-MR antibody (clone ID5 from Gomez-Sanchez, 1:500). A Zeiss laser scanning confocal microscope (LSM 880; Carl Zeiss) was used to analyze protein–protein interactions. To quantify the PLA signals (aka puncta), maximum intensity projections of the raw images were split into single channel images by MetaMorph software (Molecular devices; https://www.moleculardevices.com/products/cellular-imaging-systems/high-content-analysis/metamorph-microscopy).

Analysis of plasma membrane integrity by flow cytometry

Plasma membrane integrity was measured by adding PI (Thermo Fisher Scientific) to live cells at a final concentration of 10 ug/ml immediately prior to flow cytometric analysis. Ten thousand single cells were analyzed using a BD LSRFortessa flow cytometer equipped with FACSDiva (https://www.bdbiosciences.com/en-us/products/software/instrument-software/bd-facsdiva-software) software. Cells were excited with a 561 nm laser and PI fluorescence was detected at 585 nm. A gate was drawn on a PI histogram for the control sample to determine the percent of viable and dead cells and projected onto a forward-scatter *versus* PI contour plot.

Flow cytometric analysis of annexin-V binding

Changes in membrane phosphatidylserine symmetry were determined using TACS annexin V-FITC Apoptosis Detection Kit (R&D Systems, Inc) according to the manufacturer's instructions. Briefly, cells were washed in 1X PBS and then incubated with 2 ul annexin-V FITC and PI in annexin-V binding buffer for 15 min at room temperature. After this time, the samples were diluted binding buffer and examined immediately by flow cytometry. Ten thousand single cells were analyzed using a LSRFortessa flow cytometer (Benton Dickinson) equipped with FACSDiVa software. Annexin-V FITC and PI was excited using a 488 nm and 561 nm laser and detected using a 530/30 nm and 582/15 nm filter, respectively.

siRNA experiments

siRNA knockdown of MR in MR/GR cells was performed according to previously published procedures (58, 59). MR/GR cells were seeded 24 h prior to siRNA transfection. The cells were cultured in a serum-free medium and transfected with 30 nM nontarget control siRNA or MR siRNA (SMART pool, Thermo Fisher Scientific) using Lipofectamine RNAiMAX reagent (Thermo Fisher Scientific) according to the

manufacturer's instructions. Twenty-four hours after transfection, cells were reseeded with complete medium for apoptosis flow cytometry analyses.

NanoBit assay for GR–MR heterodimer formation

Full-length coding cDNA for GR and MR, were cloned into 4 kind of vectors (pBiT1.1-C[TK/LgBiT], pBiT2.1C[TK/SmBiT], pBiT1.1-N[TK/LgBiT], and pBiT2.1-N[TK/SmBiT]) for N-terminal and C-terminal small-bit and large-bit fusion protein expressions using In-Fusion Snap Assembly master mixes (Takara). In total eight fusion protein expression vectors were constructed (Fig. 5A). HEK293 cells plated on white 96-well plates for luminescence detection were transfected with combinations of the constructed expression vectors. Forty-eight hours after the transfections, NanoBit luciferase activities were determined using Nano-Glo live-cell assay system (Promega) and GloMax Discover luminometer (Promega) for every minute in live cells. Ligands used for these assays (DEX, aldosterone, cortisol, and glucocorticoid drugs) were added after 25 min of starting luminescence detection. The final concentrations of ligands in the cell culture media were 100 nM.

Gene reporter assay

GRE2-Luc reporter (60) and phRL-tk (Promega) with pcDNA-hGR were cotransfected into HEK293 cells using Lipofectamine 3000 (Invitrogen). Twenty-four hours after the transfection, DEX (10 nM) was added to the culture media and continued culturing for the next 24 h. Luciferase activity was determined using Dual Luciferase Reporter Assay System (Promega) and relative luciferase activity in cell extracts was calculated by normalizing with Renilla luciferase activity.

ChIP-seq analysis

To profile the chromatin landscape of GR and MR in established cell lines in this study, cells were treated with vehicle *versus* Dex, and a total of 1×10^7 cells underwent cross-linking, harvesting, and sonication. The resulting sonicated chromatin was subjected to immunoprecipitation with anti-GR (D6H2L, #12041, Cell Signaling), followed by elution and reverse cross-linking. The DNA fragments obtained from each sample were then analyzed using the paired-end 75 bp sequencing protocol on either the NextSeq 500 or NovaSeq 6000 platform (Illumina) according to the manufacturer's guidelines.

For each sample, raw reads obtained from different sequencing runs were pooled together. These pooled raw reads underwent filtering based on a mean base quality score exceeding 20, and adapters were trimmed using "Trim Galore" (version 0.4, https://github.com/FelixKrueger/TrimGalore). The resulting trimmed reads were mapped to hg19 using Bowtie (61) with the parameters "-m1, -v2 –best –strata -X 1500." Afterward, aligned read files from replicate samples under each condition or treatment were merged using the "merge" function in Samtools (Version 1.3.1) (62).

Subsequently, duplicates in all merged files were eliminated using Picard (version 1.115, http://broadinstitute.github.io/picard/).

The analysis tool findPeaks from Homer (version 4.8.3) (63) was utilized to detect ChIP-seq peaks. Its principle involves pinpointing genomic regions with a higher density of sequencing reads than anticipated randomly. The pooled input sample served as a control to account for background noise during peak identification. The findPeaks was executed with parameter "-F 2 -L 0 -C 1.5 -fdr 0.001."

Upon completion of peak calling for individual samples, the combined set of identified peaks was derived by aggregating peaks called from all respective paired conditions, forming the regions eligible for quantitative comparison. The creation of a union peak list for each comparison involved two key steps: 1) consolidating two lists of peaks into a single file and organizing them in order of Chromosome coordinate and 2) merging adjacent and overlapping peaks within a 100-nt range using mergeBed, a function from bedTools (version 2.25.0) (64). Following the creation of these union peak lists, the read count for each peak in each sample was computed using coverageBed, another tool within bedTools.

The quantification results from coverageBed were imported into the Bioconductor package DESeq2 for pairwise comparisons between DMSO and DEX treated samples. Benjamini and Hochberg method was employed to correct for FDR. A peak was deemed significantly differentially bound if the FDR-adjusted *p* value was below 0.05.

All significant peaks linked to genes underwent Gene Ontology and pathway analyses *via* GREAT (version 3.0.0) (65). Additionally, motif analysis was performed using findMotifsGenome.pl from Homer, utilizing default parameters.

Heat map was created utilizing Deeptools (V2.4.2) (66).

ChIP-qPCR

ChIP experiments were performed according to previously published procedures (58). Cells cultured on 150 mm dished were treated with DEX or vehicle for 2 h. Cross-linking of protein and DNA was achieved by 1% formaldehyde and terminated by the addition of glycine. Cells were lysed and ChIP procedures were performed using Magna ChIP kit (EMD Millipore). Isolated nuclei were subjected to sonication using a Diagenode Bioruptor (15 cycles on high setting, 30 s ON, 30 s OFF, twice). DNA shearing was evaluated on 1% agarose gels for the shear range from 200 to 1000 bp. Immunoprecipitated samples using anti-GR antibody or IgG control were isolated using the Magna ChIP kit and further purified with Qiaquick PCR purification kit (Qiagen). qPCR quantification of GR targeting area of genes identified by ChIP-seq analysis was performed using custom designed primer/probes shown in Table S4.

MD simulation

The starting configurations of the LBDs of GR and the MR for the MD trajectories were from PDB IDs 1M2Z and 6UDA, respectively. In the X-ray structures, both GR (residues

512–777) and MR (residues 738–983) had DEX as the associated ligand. Missing residues 910 to 913 of MR were added using the program Modeller10.2 and its bound ligand (DEX) was replaced by aldosterone. The two monomers were aligned using the MR dimer template in PDB ID 2AB2. This was mainly due to the fact that the nanobit assay points to the C termini being in a close proximity. Using the Leap module of Amber.20, protons and missing side chains were introduced to the dimer system and then the dimer was solvated in a box of TIP3P water with the box boundary selected to be extended 20 Å from the nearest protein atom. All Lys, Arg, Glu, and Asp residues are in their charged states. Histidine residues were deemed ε-protonated. Seventy nine Na^+ and seventy six Cl^- ions randomly replaced some of the water molecules to provide the 100 mM effective ionic concentration, while maintaining the charge neutralization. The total number of water molecules in the system was 41,340, resulting a total of 132,508 atoms in the simulation box. Prior to equilibration, each solvated system was sequentially subjected to 1) 500 ps belly dynamics with fixed peptide, 2) minimization (5000 steps), 3) constant temperature (200 K), constant pressure (1 atm) dynamics ($\sim$1 ns) at fixed protein to assure a reasonable starting density around 1 g/cc, 4) minimization (5000 steps), 5) step-wise heating MD at constant volume (to bring the temperature up to 300K in 3 ns), and 6) constant volume simulation for 10 ns with a constraint force constant of 10 kcal/mol applied only on backbone heavy atoms. After releasing all constraining forces within the next 20 ns of the equilibration period, sampling was increased by performing three independent, constant-temperature (Langevin thermostat) constant-volume MD simulations for 1.2 μs each. All trajectories were calculated using the PMEMD module of Amber.20 with 2 fs time step. Long range coulombic interactions were handled using the PME method with a 10 Å cutoff for the direct interactions. The amino acid parameters were selected from the FF14SB force field of Amber.20, and the parameters used for DEX and aldosterone were given in the Tables S5 and S6. At the salt concentration of 100 mM, the MMGBSA module with the standard parameters was used to estimate interaction energies of the residues from 1200 samples selected from MD simulations at each nanosecond interval. Only two trajectories with small total RMSDs (<5 Å) from the starting conformations were used in this analysis.

Statistical analysis

Statistical analyses were performed using GraphPad Prism (version 8.3.0, GraphPad Software; https://www.graphpad.com/features). All data were presented as means ± SD. Student's *t* test and one- and two-way ANOVA were employed according to the number of groups and comparisons. Significant differences between two groups by two-way ANOVA were indicated by asterisks and pound symbols (*$p < 0.05$, **$p < 0.01$, ***$p < 0.001$, ****$p < 0.0001$, and ####$p < 0.0001$)) and by Student's *t* test were indicated by pound symbols (#<0.05, ##$p < 0.01$, ###$p < 0.001$, and ####$p < 0.0001$).

Data availability

RNA-seq data and ChIP-seq data in this study are available on GEO (GSE275128) and GEO (GSE274344), respectively.

References

1. Praestholm, S. M., Correia, C. M., and Grontved, L. (2020) Multifaceted control of GR signaling and its impact on hepatic transcriptional networks and metabolism. *Front. Endocrinol. (Lausanne)* **11**, 572981
2. Vegiopoulos, A., and Herzig, S. (2007) Glucocorticoids, metabolism and metabolic diseases. *Mol. Cell Endocrinol.* **275**, 43–61
3. de Quervain, D., Schwabe, L., and Roozendaal, B. (2017) Stress, glucocorticoids and memory: implications for treating fear-related disorders. *Nat. Rev. Neurosci.* **18**, 7–19
4. Uchoa, E. T., Aguilera, G., Herman, J. P., Fiedler, J. L., Deak, T., and de Sousa, M. B. (2014) Novel aspects of glucocorticoid actions. *J. Neuroendocrinol.* **26**, 557–572
5. Raulo, A., and Dantzer, B. (2018) Associations between glucocorticoids and sociality across a continuum of vertebrate social behavior. *Ecol. Evol.* **8**, 7697–7716
6. Suh, S., and Park, M. K. (2017) Glucocorticoid-induced diabetes mellitus: an important but overlooked problem. *Endocrinol. Metab. (Seoul)* **32**, 180–189

7. Cain, D. W., and Cidlowski, J. A. (2017) Immune regulation by glucocorticoids. *Nat. Rev. Immunol.* **17**, 233–247

8. Diaz-Jimenez, D., Kolb, J. P., and Cidlowski, J. A. (2021) Glucocorticoids as regulators of macrophage-mediated tissue homeostasis. *Front. Immunol.* **12**, 669891

9. Cohen, D. M., and Steger, D. J. (2017) Nuclear receptor function through genomics: lessons from the glucocorticoid receptor trends. *Endocrinol Metab.* **28**, 531–540

10. Frigo, D. E., Bondesson, M., and Williams, C. (2021) Nuclear receptors: from molecular mechanisms to therapeutics. *Essays Biochem.* **65**, 847–856

11. Weikum, E. R., Knuesel, M. T., Ortlund, E. A., and Yamamoto, K. R. (2017) Glucocorticoid receptor control of transcription: precision and plasticity via allostery. *Nat. Rev. Mol. Cell Biol.* **18**, 159–174

12. Oakley, R. H., and Cidlowski, J. A. (2011) Cellular processing of the glucocorticoid receptor gene and protein: new mechanisms for generating tissue-specific actions of glucocorticoids. *J. Biol. Chem.* **286**, 3177–3184

13. Quatrini, L., and Ugolini, S. (2021) New insights into the cell- and tissue-specificity of glucocorticoid actions. *Cell Mol. Immunol.* **18**, 269–278

14. Altonsy, M. O., Sasse, S. K., Phang, T. L., and Gerber, A. N. (2014) Context-dependent cooperation between nuclear factor kappaB (NF-kappaB) and the glucocorticoid receptor at a TNFAIP3 intronic enhancer: a mechanism to maintain negative feedback control of inflammation. *J. Biol. Chem.* **289**, 8231–8239

15. Syed, A. P., Greulich, F., Ansari, S. A., and Uhlenhaut, N. H. (2020) Anti-inflammatory glucocorticoid action: genomic insights and emerging concepts. *Curr. Opin. Pharmacol.* **53**, 35–44

16. Butz, H., and Patocs, A. (2022) Mechanisms behind context-dependent role of glucocorticoids in breast cancer progression. *Cancer Metastasis Rev.* **41**, 803–832

17. Huzard, D., Rappeneau, V., Meijer, O. C., Touma, C., Arango-Lievano, M., Garabedian, M. J., *et al.* (2021) Experience and activity-dependent control of glucocorticoid receptors during the stress response in large-scale brain networks. *Stress* **24**, 130–153

18. Cruz-Topete, D., and Cidlowski, J. A. (2015) One hormone, two actions: anti- and pro-inflammatory effects of glucocorticoids. *Neuroimmunomodulation* **22**, 20–32

19. Cruz-Topete, D., Oakley, R. H., Carroll, N. G., He, B., Myers, P. H., Xu, X., *et al.* (2019) Deletion of the cardiomyocyte glucocorticoid receptor leads to sexually dimorphic changes in cardiac gene expression and progression to heart failure. *J. Am. Heart Assoc.* **8**, e011012

20. Trapp, T., Rupprecht, R., Castren, M., Reul, J. M., and Holsboer, F. (1994) Heterodimerization between mineralocorticoid and glucocorticoid receptor: a new principle of glucocorticoid action in the CNS. *Neuron* **13**, 1457–1462

21. Liu, W., Wang, J., Sauter, N. K., and Pearce, D. (1995) Steroid receptor heterodimerization demonstrated in vitro and in vivo. *Proc. Natl. Acad. Sci. U. S. A.* **92**, 12480–12484

22. Savory, J. G., Prefontaine, G. G., Lamprecht, C., Liao, M., Walther, R. F., Lefebvre, Y. A., *et al.* (2001) Glucocorticoid receptor homodimers and glucocorticoid-mineralocorticoid receptor heterodimers form in the cytoplasm through alternative dimerization interfaces. *Mol. Cell Biol.* **21**, 781–793

23. Derfoul, A., Robertson, N. M., Lingrel, J. B., Hall, D. J., and Litwack, G. (1998) Regulation of the human Na/K-ATPase beta1 gene promoter by mineralocorticoid and glucocorticoid receptors. *J. Biol. Chem.* **273**, 20702–20711

24. Kiilerich, P., Triqueneaux, G., Christensen, N. M., Trayer, V., Terrien, X., Lombès, M., *et al.* (2015) Interaction between the trout mineralocorticoid and glucocorticoid receptors. *J. Mol. Endocrinol.* **55**, 55–68

25. Mifsud, K. R., Kennedy, C. L. M., Salatino, S., Sharma, E., Price, E. M., Haque, S. N., *et al.* (2021) Distinct regulation of hippocampal neuroplasticity and ciliary genes by corticosteroid receptors. *Nat. Commun.* **12**, 4737

26. Mifsud, K. R., and Reul, J. M. (2016) Acute stress enhances heterodimerization and binding of corticosteroid receptors at glucocorticoid target genes in the hippocampus. *Proc. Natl. Acad. Sci. U. S. A.* **113**, 11336–11341

27. Bigas, J., Sevilla, L. M., Carceller, E., Boix, J., and Perez, P. (2018) Epidermal glucocorticoid and mineralocorticoid receptors act cooperatively to regulate epidermal development and counteract skin. *Inflammation Cell Death Dis.* **9**, 588

28. Le Billan, F., Amazit, L., Bleakley, K., Xue, Q. Y., Pussard, E., Lhadj, C., *et al.* (2018) Corticosteroid receptors adopt distinct cyclical transcriptional signatures. *FASEB J.* **32**, 5626–5639

29. Rivers, C. A., Rogers, M. F., Stubbs, F. E., Conway-Campbell, B. L., Lightman, S. L., and Pooley, J. R. (2019) Glucocorticoid receptor-tethered mineralocorticoid receptors increase glucocorticoid-induced transcriptional responses. *Endocrinology* **160**, 1044–1056

30. Pooley, J. R., Rivers, C. A., Kilcooley, M. T., Paul, S. N., Cavga, A. D., Kershaw, Y. M., *et al.* (2020) Beyond the heterodimer model for mineralocorticoid and glucocorticoid receptor interactions in nuclei and at DNA. *PLoS One* **15**, e0227520

31. Carceller-Zazo, E., Sevilla, L. M., Pons-Alonso, O., Chiner-Oms, A., Amazit, L., An Vu, T., *et al.* (2023) The mineralocorticoid receptor modulates timing and location of genomic binding by glucocorticoid receptor in response to synthetic glucocorticoids in keratinocytes. *FASEB J.* **37**, e22709

32. Oakley, R. H., Cruz-Topete, D., He, B., Foley, J. F., Myers, P. H., Xu, X., *et al.* (2019) Cardiomyocyte glucocorticoid and mineralocorticoid receptors directly and antagonistically regulate heart disease in mice. *Sci. Signal.* **12**, eaau9685

33. Oakley, R. H., Whirledge, S. D., Petrillo, M. G., Riddick, N. V., Xu, X., Moy, S. S., *et al.* (2021) Combinatorial actions of glucocorticoid and mineralocorticoid stress hormone receptors are required for preventing neurodegeneration of the mouse Hippocampus. *Neurobiol. Stress* **15**, 100369

34. Cruz-Topete, D., Oakley, R. H., and Cidlowski, J. A. (2020) Glucocorticoid signaling and the aging heart. *Front. Endocrinol. (Lausanne)* **11**, 347

35. Oakley, R. H., Riddick, N. V., Moy, S. S., and Cidlowski, J. A. (2024) Imbalanced glucocorticoid and mineralocorticoid stress hormone receptor function has sex-dependent and independent regulatory effects in the mouse Hippocampus. *Neurobiol. Stress* **28**, 100589

36. Lu, N. Z., Collins, J. B., Grissom, S. F., and Cidlowski, J. A. (2007) Selective regulation of bone cell apoptosis by translational isoforms of the glucocorticoid receptor. *Mol. Cell Biol.* **27**, 7143–7160

37. Bledsoe, R. K., Madauss, K. P., Holt, J. A., Apolito, C. J., Lambert, M. H., Pearce, K. H., *et al.* (2005) A ligand-mediated hydrogen bond network required for the activation of the mineralocorticoid receptor. *J. Biol. Chem.* **280**, 31283–31293

38. Dougherty, E. J., Elinoff, J. M., Ferreyra, G. A., Hou, A., Cai, R., Sun, J., *et al.* (2016) Mineralocorticoid receptor (MR) trans-activation of inflammatory AP-1 signaling: dependence on DNA sequence, MR conformation, and AP-1 family member expression. *J. Biol. Chem.* **291**, 23628–23644

39. Rupprecht, R., Arriza, J. L., Spengler, D., Reul, J. M., Evans, R. M., Holsboer, F., *et al.* (1993) Transactivation and synergistic properties of the mineralocorticoid receptor: relationship to the glucocorticoid receptor. *Mol. Endocrinol.* **7**, 597–603

40. Soderberg, O., Gullberg, M., Jarvius, M., Ridderstrale, K., Leuchowius, K. J., Jarvius, J., *et al.* (2006) Direct observation of individual endogenous protein complexes in situ by proximity ligation. *Nat. Methods* **3**, 995–1000

41. Dixon, A. S., Schwinn, M. K., Hall, M. P., Zimmerman, K., Otto, P., Lubben, T. H., *et al.* (2016) NanoLuc complementation reporter optimized for accurate measurement of protein interactions in cells. *ACS Chem. Biol.* **11**, 400–408

42. Schena, M., Freedman, L. P., and Yamamoto, K. R. (1989) Mutations in the glucocorticoid receptor zinc finger region that distinguish interdigitated DNA binding and transcriptional enhancement activities. *Genes Dev.* **3**, 1590–1601

43. Funder, J. W. (1997) Glucocorticoid and mineralocorticoid receptors: biology and clinical relevance. *Annu. Rev. Med.* **48**, 231–240

44. Hudson, W. H., Youn, C., and Ortlund, E. A. (2014) Crystal structure of the mineralocorticoid receptor DNA binding domain in complex with DNA. *PLoS One* **9**, e107000

45. Ou, X. M., Storring, J. M., Kushwaha, N., and Albert, P. R. (2001) Heterodimerization of mineralocorticoid and glucocorticoid receptors at a novel negative response element of the 5-HT1A receptor gene. *J. Biol. Chem.* **276**, 14299–14307

46. Planey, S. L., Derfoul, A., Steplewski, A., Robertson, N. M., and Litwack, G. (2002) Inhibition of glucocorticoid-induced apoptosis in 697 pre-B lymphocytes by the mineralocorticoid receptor N-terminal domain. *J. Biol. Chem.* **277**, 42188–42196

47. Oakley, R. H., and Cidlowski, J. A. (2013) The biology of the glucocorticoid receptor: new signaling mechanisms in health and disease. *J. Allergy Clin. Immunol.* **132**, 1033–1044

48. Galliher-Beckley, A. J., and Cidlowski, J. A. (2009) Emerging roles of glucocorticoid receptor phosphorylation in modulating glucocorticoid hormone action in health and disease. *IUBMB Life* **61**, 979–986

49. Duma, D., Jewell, C. M., and Cidlowski, J. A. (2006) Multiple glucocorticoid receptor isoforms and mechanisms of post-translational modification. *J. Steroid Biochem. Mol. Biol.* **102**, 11–21

50. Vandevyver, S., Dejager, L., and Libert, C. (2014) Comprehensive overview of the structure and regulation of the glucocorticoid receptor. *Endocr. Rev.* **35**, 671–693

51. Petta, I., Dejager, L., Ballegeer, M., Lievens, S., Tavernier, J., De Bosscher, K., *et al.* (2016) The interactome of the glucocorticoid receptor and its influence on the actions of glucocorticoids in combatting inflammatory and infectious diseases. *Microbiol. Mol. Biol. Rev.* **80**, 495–522

52. Jewell, C. M., Scoltock, A. B., Hamel, B. L., Yudt, M. R., and Cidlowski, J. A. (2012) Complex human glucocorticoid receptor dim mutations define glucocorticoid induced apoptotic resistance in bone cells. *Mol. Endocrinol.* **26**, 244–256

53. Uphoff, C. C., and Drexler, H. G. (2011) Detecting mycoplasma contamination in cell cultures by polymerase chain reaction Methods. *Mol. Biol.* **731**, 93–103

54. Dobin, A., Davis, C. A., Schlesinger, F., Drenkow, J., Zaleski, C., Jha, S., *et al.* (2013) STAR: ultrafast universal RNA-seq aligner. *Bioinformatics* **29**, 15–21

55. Liao, Y., Smyth, G. K., and Shi, W. (2013) The Subread aligner: fast, accurate and scalable read mapping by seed-and-vote. *Nucleic Acids Res.* **41**, e108

56. Love, M. I., Huber, W., and Anders, S. (2014) Moderated estimation of fold change and dispersion for RNA-seq data with DESeq2. *Genome Biol.* **15**, 550

57. Gomez-Sanchez, C. E., de Rodriguez, A. F., Romero, D. G., Estess, J., Warden, M. P., Gomez-Sanchez, M. T., *et al.* (2006) Development of a panel of monoclonal antibodies against the mineralocorticoid receptor. *Endocrinology* **147**, 1343–1348

58. Petrillo, M. G., Oakley, R. H., and Cidlowski, J. A. (2019) beta-Arrestin-1 inhibits glucocorticoid receptor turnover and alters glucocorticoid signaling. *J. Biol. Chem.* **294**, 11225–11239

59. Ren, R., Oakley, R. H., Cruz-Topete, D., and Cidlowski, J. A. (2012) Dual role for glucocorticoids in cardiomyocyte hypertrophy and apoptosis. *Endocrinol.* **153**, 5346–5360

60. Wallace, A. D., and Cidlowski, J. A. (2001) Proteasome-mediated glucocorticoid receptor degradation restricts transcriptional signaling by glucocorticoids. *J. Biol. Chem.* **276**, 42714–42721

61. Langmead, B., Trapnell, C., Pop, M., and Salzberg, S. L. (2009) Ultrafast and memory-efficient alignment of short DNA sequences to the human genome. *Genome Biol.* **10**, R25

62. Li, H., Handsaker, B., Wysoker, A., Fennell, T., Ruan, J., Homer, N., *et al.* (2009) The sequence alignment/map format and SAMtools. *Bioinformatics* **25**, 2078–2079

63. Heinz, S., Benner, C., Spann, N., Bertolino, E., Lin, Y. C., Laslo, P., *et al.* (2010) Simple combinations of lineage-determining transcription factors prime cis-regulatory elements required for macrophage and B cell identities. *Mol. Cell* **38**, 576–589

64. Quinlan, A. R., and Hall, I. M. (2010) BEDTools: a flexible suite of utilities for comparing genomic features. *Bioinformatics* **26**, 841–842

65. McLean, C. Y., Bristor, D., Hiller, M., Clarke, S. L., Schaar, B. T., Lowe, C. B., *et al.* (2010) GREAT improves functional interpretation of cis-regulatory regions. *Nat. Biotechnol.* **28**, 495–501

66. Ramirez, F., Ryan, D. P., Gruning, B., Bhardwaj, V., Kilpert, F., Richter, A. S., *et al.* (2016) deepTools2: a next generation web server for deep-sequencing data analysis. *Nucleic Acids Res.* **44**, W160–W165